12-2019

Optimizing composition in MnBi permanent magnet alloys

Brandt A. Jensen
Ames Laboratory

Wei Tang
Ames Laboratory, weitang@ameslab.gov

Xubo Liu
Ames Laboratory, liux@ameslab.gov

Alexandra I. Nolte
Ames Laboratory

Gaoyuan Ouyang
Iowa State University and Ames Laboratory, gaoyuan@ameslab.gov

See next page for additional authors

Optimizing composition in MnBi permanent magnet alloys

Abstract

MnBi is an attractive rare-earth-free permanent magnetic material due to its low materials cost, high magnetocrystalline anisotropy (1.6 × 106 J m−3), and good magnetization (81 emu g−1) at room temperature. Although the theoretical maximum energy product (BH)max of 20 MGOe is lower than that of NdFeB-based magnets, the low temperature phase (LTP) of MnBi has a positive temperature coefficient of coercivity, up to 200 °C, which makes it a potential candidate for high temperature applications such as permanent magnet motors. However, the oxygen sensitivity of the MnBi compound and the peritectic reaction between Mn and Bi make it difficult to synthesize into a material with high purity. This challenge is partly offset by adding excess Mn to the alloy, with composition close to Mn55Bi45 resulting in the highest saturation magnetization after common processing techniques such as arc melting, casting, melt spinning, and ball milling. Here we report a systematic process which reduces the amount of excessive Mn, while simultaneously providing a large saturation magnetization (MS) of 79 emu g−1 at 300 K in the annealed Mn52Bi48 ribbons. We also report excellent magnetic properties in the ball powders, resulting in 0.5–5 μm particles with MS of 75.5 emu g−1, coercivity Hci of 10.8 kOe, and (BH)max of 13 MGOe using 9 T applied field at 300 K. A secondary annealing treatment on various ball milled powders increased Hci by up to 21%, and also resulted in an increase in MS up to 78.8 emu g−1.

Keywords

Non-rare-earth, Permanent magnet, MnBi

Disciplines

Materials Science and Engineering

Authors

Brandt A. Jensen, Wei Tang, Xubo Liu, Alexandra I. Nolte, Gaoyuan Ouyang, Kevin W. Dennis, and Jun Cui

Optimizing Composition in MnBi Permanent Magnet Alloys

B.A. Jensen[1], A. Nolte[1], W. Tang,[1] X. B. Liu[1], G. Ouyang[1,2], K. W. Dennis,[1] J. Cui[1,2]

[1]Division of Materials Sciences and Engineering, Ames Laboratory, Ames, IA

[2]Department of Materials Science and Engineering, Iowa State University, Ames, IA

Abstract:

MnBi is an attractive rare-earth-free permanent magnetic material due to its low materials cost, high magnetocrystalline anisotropy (1.6×10^6 J m^{-3}), and good magnetization (81 emu g^{-1}) at room temperature. Although the theoretical maximum energy product $(BH)_{max}$ of 20 MGOe is lower than that of NdFeB-based magnets, the low temperature phase (LTP) of MnBi has a positive temperature coefficient of coercivity, up to 200 °C, which makes it a potential candidate for high temperature applications such as permanent magnet motors. However, the oxygen sensitivity of the MnBi compound and the peritectic reaction between Mn and Bi make it difficult to synthesize into a material with high purity. This challenge is partly offset by adding excess Mn to the alloy, with composition close to $Mn_{55}Bi_{45}$ resulting in the highest saturation magnetization after common processing techniques such as arc melting, casting, melt spinning, and ball milling. Here we report a systematic process which reduces the amount of excessive Mn, while simultaneously providing a large saturation magnetization (M_S) of 79 emu g^{-1} at 300 K in the annealed $Mn_{52}Bi_{48}$ ribbons. We also report excellent magnetic properties in the ball powders, resulting in 0.5-5 μm particles with M_S of 75.5 emu g^{-1}, coercivity H_{ci} of 10.8 kOe, and $(BH)_{max}$ of 13 MGOe using 9 T applied field at 300 K. A secondary annealing treatment on various ball milled powders increased H_{ci} by up to 21%, and also resulted in an increase in M_S up to 78.8 emu g^{-1}.

1. Introduction

The low temperature phase of MnBi (LTP-MnBi) is a hard magnetic material potentially suitable for use in permanent magnet motors due to its high magnetocrystalline anisotropy (1.6×10^6 J m^{-3}) [1] and good saturation magnetization (81 emu g^{-1}) at room temperature [2]. LTP-MnBi is a peritectic compound that exhibits a first-order structural transition between the temperatures of 340 °C and 355 °C, at which point it transforms into the paramagnetic high temperature phase [3][4][5]. Trouble arises when trying to form LTP-MnBi from the melt due to the high temperature of the liquidus for the stoichiometric MnBi composition [6][7], which results in primary solidification of Mn accompanied with a large amount of phase segregation from the remaining Bi-rich liquid. Due to the sluggish kinetics of Mn atoms below the LTP-MnBi decomposition temperature of 355°C [8], as well as the oxygen sensitivity of the Mn-Bi system [9][10], it has proven difficult to obtain phase pure materials with traditional processing techniques.

To combat the phase segregation of Mn from the melt during conventional processing techniques such as arc melting, casting, melt spinning, or sintering, an excess amount of Mn is often added to the alloy to maximize the phase fraction of LTP-MnBi. About 4 at.% excessive Mn is needed to first form the high temperature $Mn_{1.08}Bi$ phase, which exists in the temperature range from 340 to 446 °C and is found difficult to by-pass with conventional processing methods [2][10][11][12][13][14][15][16][17][18]. This excess Mn increases the volume fraction of LTP-MnBi in practice, but ultimately dilutes the potential magnetic properties unless this waste material can be removed with yet another processing step (i.e. magnetic separation

[12][16][17][19]). Furthermore, in order to take advantage of the large magnetocrystalline anisotropy of the MnBi system, it is necessary to break the polycrystalline MnBi particle apart till it becomes single crystal. In practice this is usually achieved through ball milling. However, even low energy ball milling was found to be energetic enough for inducing the decomposition of the LTP-MnBi phase into Mn and Bi [11][15][20]. Cryomilling mitigates the decomposition issue to certain degree, but can't completely solve it [11][21]. This decomposition reaction further reduces the phase fraction of LTP-MnBi in the powders materials, lowering M_S even further.

Traditional metallurgical processes are preferred in order to maintain cost effectiveness of the manufacturing process. Techniques such as cryomilling or magnetic separation should be avoided. Identifying methods to increase the LTP-MnBi phase without the use of expensive or time-consuming techniques is of great interest in the magnetics community. In this report we expand upon our previous work which identified an optimum MnBi composition by using a more refined processing technique. Processing adjustments have been made which result in a greater phase fraction of LTP-MnBi in the high-performance ribbons and powders.

2. Experimental

2.1 Sample preparation

High-purity Mn (Ames Lab MPC) and Bi shot (Aldrich: 99.999% metals basis) were weighed according to the designed atomic ratio, then arc melted under a partial pressure of ultra-high purity argon. The samples were flipped and re-melted 5 times to ensure homogeneity. Mass losses were kept to less than 0.3 wt.% during the arc melting process. The ingots were placed into a quartz crucible fitted with a 0.81 mm precision capillary orifice, then melt spun in 1/3 atm. ultra-high purity helium with an overpressure of 120 Torr and a wheel speed of 12 m/s. The

ribbons were packed into a tantalum tube which was then sealed inside a quartz ampoule with a partial pressure of ultra-high purity argon. The MnBi ribbons were annealed at 290°C for five days and allowed to air cool. The ribbons were transferred to a nitrogen dry box and ground into a coarse powder (< 425 µm) with mortar and pestle. The coarse powder was loaded into a 2.5" hardened steel vial with cyclohexane, using 440 stainless steel milling media in a 20:1 weight ratio. The dimensions of the milling media were 1/4" and 3/8" in diameter. The powders were milled for 7-10 hours and then transferred into a nitrogen dry box where the cyclohexane was decanted.

Magnetic characterization was performed using a Quantum Design PPMS® DynaCool™ with a vibrating sample magnetometer (VSM) option installed. The ground ribbon pieces and ball milled powders were randomly packed and measured at T = 300 K with a maximum applied magnetic field of $\mu_0 H = 9$ T for M_S measurements. Powders were heated to T = 335 K and aligned in wax with a field of $\mu_0 H = 9$ T, then allowed to cool to room temperature for $(BH)_{max}$ measurements. The measured magnetic moment was divided by the actual weight of the powder to obtain the magnetization. The resulted MH curves were not corrected for any demagnetization factor due to the uncertainty of the magnetostatic interaction among powders. MnBi powders and annealed ribbon pieces were imaged using a FEI Teneo field-emission scanning electron microscope (FE-SEM) equipped with an Oxford Aztec energy dispersive detector (EDS). An accelerating voltage of 15 kV was used for all EDS work. X-ray diffraction (XRD) was performed with a Bruker D8 Advance (Cu K_α radiation, $\lambda = 1.54056$ Å) diffractometer in the $\theta/2\theta$ mode with the following parameters: 2θ region of 20 – 90°, step size of 0.02°, collection time of 1.5 s/step. Rietveld refinement was performed using GSAS software in order to determine phase fractions and lattice

parameters. Composition of annealed melt spun ribbons were analyzed by EAG Laboratories using inductively coupled plasma atomic emission spectroscopy (ICP-AES).

3. Experimental Results

3.1. Saturation magnetization of MnBi ribbons and powders

M_S values of the annealed ribbons and ball milled powders are shown in Figure 1. The ribbon samples show a clear peak of 79 emu g^{-1} at the nominal composition of $Mn_{52}Bi_{48}$. On average, the magnetization of the samples drop 4% after milling for 8 hours. The cause for the drop in magnetization is primarily due to the decomposition of LTP-MnBi into elemental Mn and Bi which is discussed below. The magnetization trend of the ball milled powders is similar to the melt spun ribbons, with the $Mn_{52}Bi_{48}$ alloy also having the highest magnetization. This is about 3% less of Mn comparing to our previous work.[10]

3.2 Effect of heat treatment on composition of $Mn_{52}Bi_{48}$ ribbon

Backscattered SEM micrographs of the annealed $Mn_{52}Bi_{48}$ ribbons are shown in Figures 2 and 3. The grain sizes of the annealed ribbons were between 2 – 20 μm, with slightly larger grains appearing on the free side of the ribbon pieces. A few clusters of Mn grains were detected on the wheel side surface of the ribbons. The wheel side is the first to solidify from the melt, so the primary solidification of Mn is expected to take place here. No grains of Mn were detected on the free side of the ribbon surfaces, and no grains of Bi were detected on either surface of the ribbons. A few regions that were rich in Mn content were scanned and analyzed using ImageJ software. Figure 3 is an example of such a region, with the calculated area fraction of 1% Mn for

this selected area. EDS was performed over large areas of the ribbon surface which resulted in compositions of $Mn_{50}Bi_{50}$ to within a fraction of a percent.

Figure 4 shows the XRD pattern for the $Mn_{52}Bi_{48}$ annealed ribbon pieces. From the Rietveld refinement the annealed ribbons are nearly phase pure, containing 98.2 wt.% LTP-MnBi, 0.5 wt.% Bi, and 1.2 wt.% MnO_2. The calculated weight fractions of both Bi and MnO_2 present in the ribbons are close to the error in the analysis. Although grains of Mn were detected in SEM, the amount of Mn present was below the detection limits of XRD analysis.

ICP-AES was conducted on the annealed $Mn_{52}Bi_{48}$ ribbons to support XRD and EDS chemical analysis. The compositions and uncertainties are shown in Table 1. There was approximately 2 at.% oxidation within the annealed ribbons, so the results for Mn and Bi atomic concentration have been normalized to 100%. The annealed ribbons were exposed to air for approximately 30 minutes as the sample was being prepared, so some of this oxidation was possibly a result from the sample preparation. Four replicate measurements were taken for this sample, and the variation between the replicates produced a global expanded uncertainty of less than 0.5 at.%. The chemistry of $Mn_{50.94}Bi_{49.06}$ was determined for annealed ribbons, which is in close agreement with both XRD and SEM-EDS analysis.

3.3 Effect of ball milling time and post-mill annealing on MnBi powders

Low energy ball milling of MnBi coarse powder typically produces particles with two size ranges: one from 2.41-4.13 mm and other from 0.43-0.68 mm. For the batch of powders milled for 7 hours, the bimodal particles sizes are (0.59 ± 0.20 mm and 3.43 ± 0.82 mm). For the powders milled for 8, 9 and 10 hours, the corresponding particle bimodal sizes are (0.57 ± 0.22

mm and 2.66 ± 0.80 mm), (0.51 ± 0.23 mm and 2.46 ± 0.77 mm), and (0.43 ± 0.17 mm and 2.41 ± 0.83 mm), respectively.

Effects of ball milling time on the magnetic properties of wax-aligned $Mn_{52}Bi_{48}$ powders are shown Figure 5 and listed in Table 2. As expected, coercivity increases as the length of milling time increases. The powders which were ball milled for the maximum time of 10 hours show the highest coercivity at 12.3 kOe. This increase in coercivity is generally accompanied with a drop in magnetization. The squareness M_r/M_S and $(BH)_{max}$ of the powders peak at 8 hours of ball milling time.

The powder samples which were milled for either 7 or 10 hours were then annealed at 290°C and re-measured in identical conditions. The effects of the post-mill annealing treatment are shown in Figure 6 and listed in Table 2. The annealing treatment increased coercivity in both samples, with a more significant effect in the powders milled for 10 hours. The coercivity of the annealed powders which were ball milled for 10 hours was 15.0 kOe, which is a 22% increase compared to the value of 12.3 kOe in the as-milled powder. The coercivity of the powders which were milled for 7 hours increased by 6% after annealing. The magnetization of the powders milled for 10 hours dropped from 71.8 emu g^{-1} to 70.7 emu g^{-1} after the heat treatment, a reduction of about 1.5%. However, the magnetization increased from 72.8 emu g^{-1} to 78.8 emu g^{-1} for the powders which were milled for 7 hours and then annealed, approaching the theoretical saturation magnetization. The ratio of M_r/M_S decreased for both samples upon annealing at 290°C.

SEM micrographs of $Mn_{52}Bi_{48}$ powders which were ball milled for 8 hours are shown in Figure 7 and Figure 8. The particle sizes of the milled powders were between 0.5 – 5 μm and were seemingly independent of the chemistries explored in this experiment. EDS measurements were

taken on individual grains which happened to be both flat and normal to the beam current, and area scans on multiple compositions were also performed. A few grains of both elemental Mn and Bi were detected in every sample. The Mn grains, shown in Figure 8a, were consistently small and sometimes embedded within larger particles of MnBi. Individual grains of Bi, shown in Figure 8b, were typically 15 – 20 μm in size, and there were also some Bi-rich grains as expected. All EDS area scans were close to $Mn_{50}Bi_{50}$ in composition. The size of the powder particles milled for 8 hours are mostly ≤ 5 μm, which is sufficiently small to obtain large values of coercivity. There was no evidence of contamination from the ball milling apparatus in the form of Fe-rich particles.

XRD analysis was performed on the $Mn_{52}Bi_{48}$ alloy throughout the process, which is shown in Figure 9. The phase fractions and lattice parameters calculated from Rietveld refinement are listed in Table 3. It should be noted that the $Mn_{52}Bi_{48}$ sample discussed here is a separate sample from the $Mn_{52}Bi_{48}$ sample discussed above, however the properties of the ribbons and powders were similar. The melt spun ribbons (Fig. 9a) contained 96.9 wt.% LTP-MnBi after the annealing process, with 3.1 wt.% bismuth that was left unreacted. The bismuth content increases to 7.5 wt.% upon ball milling for 7 hours (Fig. 9b) which indicates the decomposition of LTP-MnBi. The XRD peaks for the ball milled powders broaden compared to the annealed ribbons, and the a/c ratio of the lattice parameters increases. After annealing the powders at 290°C, the XRD peaks become sharp, the a/c ratio of the lattice parameters decreases, and the LTP-MnBi phase increases to 98.5 wt.%.

3.4 Magnetic properties of aligned powder

The demagnetization curves of various wax-aligned powders are shown in Figure 10, along with values of M_S, M_r, M_r/M_S, H_{ci}, and $(BH)_{max}$ listed in Table 4. The coercivities are > 10.5 kOe for all samples, with the Bi-rich composition $Mn_{49.5}Bi_{50.5}$ showing the highest coercivity of 11.4 kOe. The samples with highest $(BH)_{max}$ are $Mn_{50.5}Bi_{49.5}$ and $Mn_{52}Bi_{48}$, two compositions closest to the 50:50 ratio. Values for $(BH)_{max}$ typically follow the same trend as M_S with the exception of $Mn_{49.5}Bi_{50.5}$, which has smaller M_S than $Mn_{53}Bi_{47}$ but larger $(BH)_{max}$ due to the better squareness in the second quadrant.

4. Discussion

Previous discussions of maximizing LTP-MnBi phase fraction using traditional processing techniques concluded the optimal starting composition to be $Mn_{55}Bi_{45}$ [10], however here we argue the optimal composition to be much closer to the stoichiometric composition. With the processing conditions described in this work, the $Mn_{52}Bi_{48}$ composition provides the highest phase fraction of LTP-MnBi in both melt spun ribbons and ball milled powders, which is to be expected if contamination is minimized throughout materials synthesis. Melt spinning the material in this current work provides a faster quench rate than the previously mentioned arc melting and casting methods. The increased quench rate finely distributes the free Mn and Bi throughout the microstructure which facilitates the reaction to form MnBi. The wheel speed was held constant in this experiment, however it may also play a role in affecting the ribbon and powder properties.

Oxidation of the MnBi alloy has also been greatly reduced during the single-step heat treatment in this work as compared to the multi-step heat treatment in our earlier work. Previously, the MnBi alloy was cast and heated to 255°C for 8 hours, then 352°C for 5 hours in a pure hydrogen atmosphere to obtain as much LTP-MnBi as possible. After this heat treatment there was still a

large amount of unreacted Mn and Bi across all compositions. The ingots were subsequently crushed, and only select powders in the range of 37 - 44 μm were further heat treated under a vacuum of 100 mTorr in order to encourage the remaining Mn and Bi to react. This second heat treatment succeeded in increasing the overall LTP-MnBi content, but it also resulted in 10-15 at.% MnO across all compositions which placed a hard limit on maximum achievable MnBi phase. The heat-treated ribbons in this updated process approached 98 wt.% MnBi as determined by mass magnetization of 79 emu g^{-1} as well as Rietveld refinement. This vacuum heat treatment consists of a single step at 290°C. Even after the decomposition of LTP-MnBi during the ball milling process in this updated work, the powders still exhibit higher magnetization and coercivity in their "as-milled" state without the need of a second heat treatment. Nonetheless, the secondary heat treatment of the powders in this work was performed under a blanket of ultra-high purity argon. This helped eliminate oxidation and increased the magnetization of the powders from 72.8 emu g^{-1} to 78.8 emu g^{-1}.

The prolonged milling times of 7-10 hours typically lead to large decreases in magnetization, remanence, and kinks in the second quadrant demagnetization curves [15], however these features are not as severe in this experiment. This is largely due to the smaller radius of the ball milling jar and smaller milling media. The energy imparted into the sample is reduced when the radius of the jar and milling media are decreased, which delays the effects of amorphization and decomposition. Some decomposition of MnBi still occurs after milling for 8 hours, which is evident from both Rietveld analysis and the 4% reduction in magnetization of the milled powders. The magnetization of 75.5 emu g^{-1} for the milled $Mn_{52}Bi_{48}$ powders (0.5 - 5 μm) reported in this experiment is still higher than the 74 emu g^{-1} for the crushed and annealed

$Mn_{55}Bi_{45}$ powders (37-44 μm) we previously reported under the same measurement conditions, with the added benefit of increased coercivity and energy product.

The trend of M_S as a function of chemistry for the powders is not as smooth as the trend in the melt spun ribbons. This may be caused by a number of factors. The magnetization curves at T = 300 K and $\mu_0 H$ = 9 T (not shown here) show that some of the packed powder samples may not have been completely saturated due to the large anisotropy of the material. Another potential factor is the difficulty in handling the highly oxygen sensitive powders. The powders are protected from oxygen during the milling process, however after the cyclohexane was decanted in a nitrogen dry box, the powders were allowed to fully dry before magnetic measurements were prepared. There may have been varying amounts of contamination during this lengthy drying process. Although the amount of MnO and MnO_2 detected from Rietveld was within the error of the measurement, a small amount of oxidation may still contribute to the noise in the data.

The coercivity of the powders is affected by multiple mechanisms as the milling time is increased. The first mechanism is the simple relationship between coercivity and powder particle size. The powder particle size decreases as the milling time increases, which increases the coercivity of the powder. The second mechanism that occurs during milling is the decomposition of the LTP-MnBi into Mn and Bi. Nonmagnetic secondary phases such as Mn and Bi may help isolate the ferromagnetic MnBi particles, leading to increases in coercivity. However, strain, plastic deformation, development of nanocrystalline structure within each particle, disordering, and amorphization of the MnBi phase may be preceding the decomposition of the MnBi phase during the milling process [22][23][24]. Both Xie et al. [11] and Cao et al. [15] have shown that low energy ball milling and surfactant assisted ball milling of $Mn_{55}Bi_{45}$ powders resulted in the formation of nanocrystalline and partially amorphous MnBi using TEM and SAED analysis. Yin

et al. detailed the evolution of the MnBi structure throughout the milling process using XRD, which included the formation of crystallites approaching 30 nm, a buildup of strain, and the rearrangement and disordering of Mn and Bi atoms within the crystal lattice [24]. The LEBM process in this present work also induces strain in the MnBi powders as evidenced by the peak broadening in the XRD pattern and the increased ratio of a/c from the lattice constants derived from Rietveld refinement. Therefore, the as-milled powders consist of a strained and disordered LTP-MnBi phase, an amorphous phase fraction, and a nanocrystalline microstructure, all of which will effect coercivity.

Annealing the $Mn_{52}Bi_{48}$ ball milled powders in this present work resulted in increased coercivity. In nucleation hardened magnetic materials such as MnBi, any lattice imperfections that result from ball milling may cause drops in H_{Ci} due to local reductions in anisotropy constants [25]. The XRD patterns of the powders ball milled for 7 hours are more broad than the annealed powders. This indicates the annealing process removed strain from the lattice and likely recrystallized the nanocrystalline powders. The XRD pattern of the annealed powders also show a phase pure material, which is complimented by the 78.8 emu g^{-1} magnetization of the powders. This indicates the 290°C post-mill annealing process reacted the decomposed Mn and Bi into LTP-MnBi. Although it cannot be determined from XRD, it is likely that the annealing treatment also converted any amorphous MnBi into a fully crystalline phase, which should result in an increase in coercivity. The annealing process will not affect the powder particle size, so this effect can be ignored.

The powders that were ball milled for 10 hours showed a 21% increase in coercivity and a 1.5% decrease in magnetization upon annealing at 290°C. The small decrease in magnetization is potentially due to partial oxidation of the MnBi powders, given their large amount of surface

area. If the decomposed Mn forms MnO, then the reaction with Bi to form LTP-MnBi becomes impossible. Another possibility for the slight decrease in magnetization is the formation of a nonmagnetic phases such as Mn_3Bi, which has been shown to crystallize from amorphous MnBi [26]. A more detailed study to determine the exact mechanism for increased coercivity upon post-mill annealing is ongoing.

In both sets of annealed powders, the 290°C post-sinter annealing process reduced the magnetic squareness of the powders. This is likely a result from neck growth of powder particles at these elevated temperatures. If a portion of powder particles are necked to each other in random orientation, the squareness of the hysteresis loop will decrease accordingly. An optimization of the post-mill annealing process may lead to phase pure MnBi powder particles without reduced squareness.

5. Conclusions

LTP-MnBi is difficult to obtain due to the peritectic nature and oxygen sensitivity of the Mn-Bi system, so an excess amount of Mn is usually added to compensate. Here we report an improved processing route that minimizes wasted Mn and reduces oxide formation, yielding LTP-MnBi that approaches 99 wt.% purity. An optimized, nominal composition of MnBi was found to be $Mn_{52}Bi_{48}$ with appropriate processing techniques and raw materials. Annealed ribbons achieved a magnetization of 79 emu g^{-1}. Powders which were ball milled for 8 hours retained a magnetization of 75.5 emu g^{-1} with a coercivity of 10.8 kOe and $(BH)_{max}$ of 13.0 MGOe. Powders which were ball milled for 10 hours retained a magnetization of 71.8 emu g^{-1} with a coercivity of 12.3 kOe. Post-mill annealing of these powders increased coercivity to 15.0 kOe with only a minor decrease in magnetization. Powders which were ball milled for 7 hours

retained a magnetization of 72.8 emu g^{-1}, and post-mill annealing increased their magnetization to 78.8 emu g^{-1}.

Acknowledgement This work was financially supported by the U.S. Department of Energy, Office of Energy Efficiency and Renewable Energy (EERE) under the Award Number EE0007794. The research was performed at Iowa State University and at Ames Laboratory, which is operated for the U.S. Department of Energy by Iowa State University under the contract number DE-AC02-07CH11358.

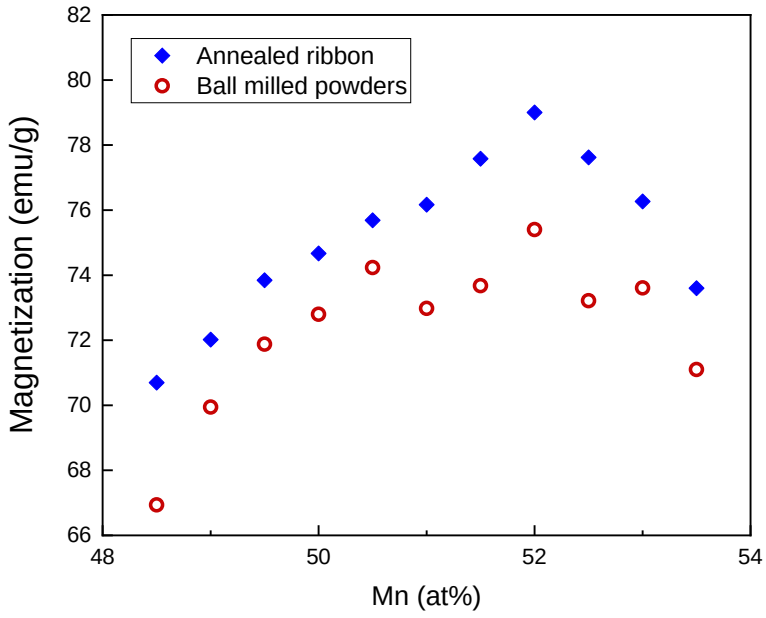

Figure 1. Room temperature saturation magnetization of $Mn_{100-x}Bi_x$ alloys. Blue data points are melt spun ribbons which were annealed at 290°C, and red data points are the resulting powders after low energy ball milling for 8 hours. Properties were measured at T = 300 K and $\mu_0 H$ = 9 T.

a) b)

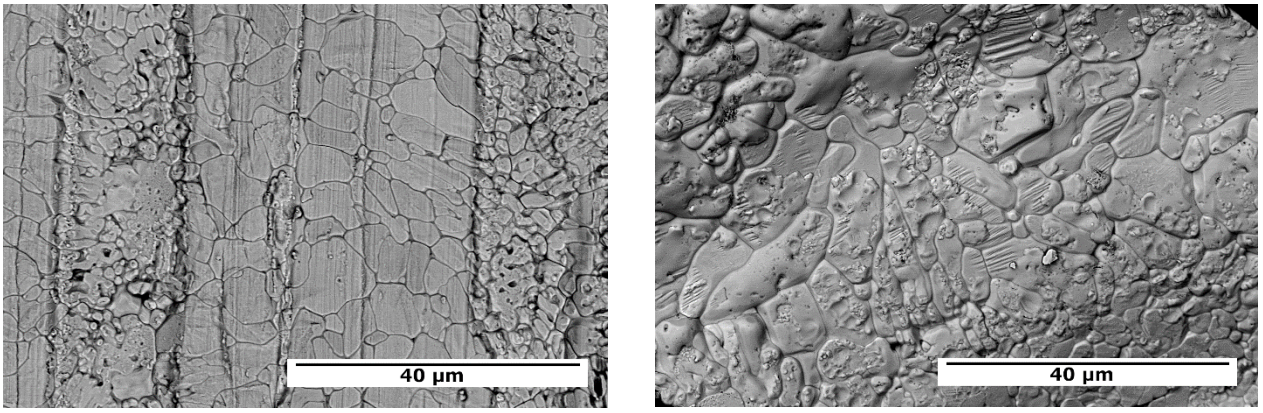

Figure 2. SEM micrograph of a) wheel side and b) free side of $Mn_{52}Bi_{48}$ ribbons after annealing at 290°C. Image was taken in backscattered electron imaging mode. Grains on wheel side are mostly phase pure and range from 2 – 15 µm. Grains on free side are phase pure and range from 2 – 20 µm.

a) b)

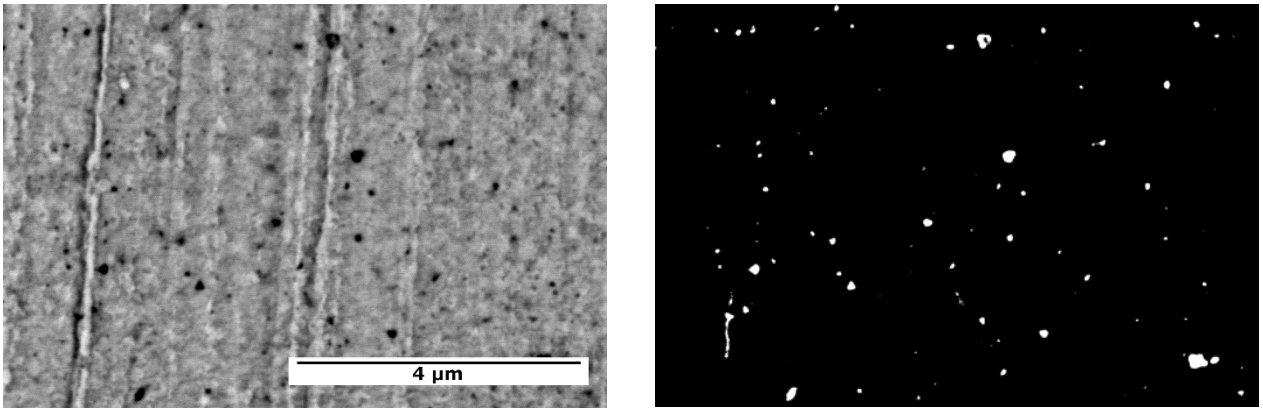

Figure 3. SEM micrograph of annealed $Mn_{52}Bi_{48}$ ribbons in a region with high concentration of Mn grains. Image a) was taken in backscattered electron imaging mode, b) depicts area fraction of Mn grains, shown in white. Mn area fraction was approximately 1% as determined using ImageJ software.

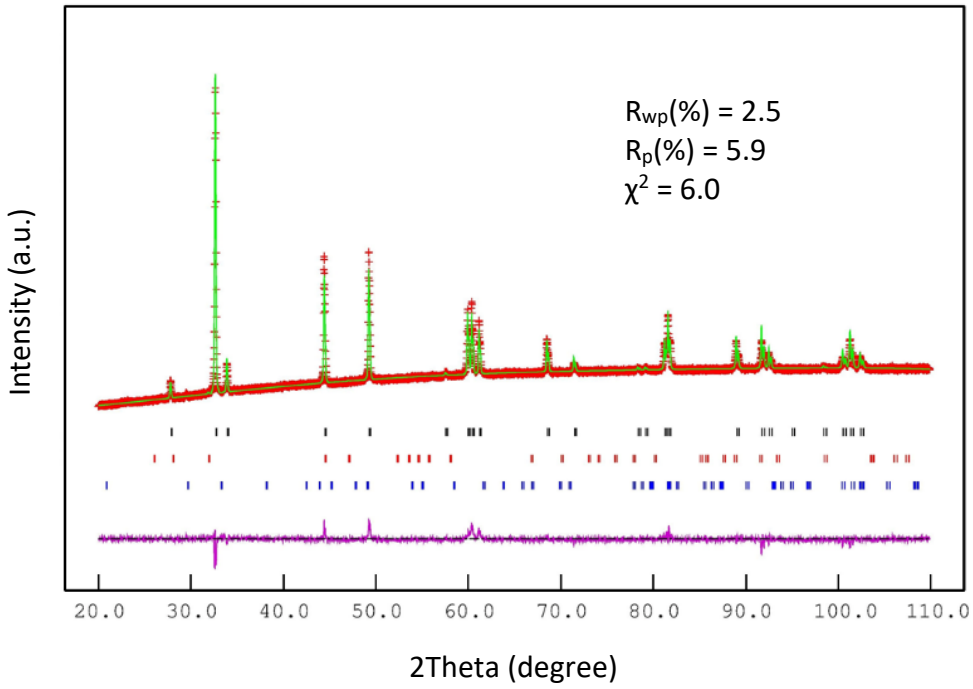

Figure 4. XRD pattern for annealed $Mn_{52}Bi_{48}$ ribbons. LTP-MnBi phase fraction was calculated to be 98.2 wt.%.

Table 1. Chemical analysis of annealed $Mn_{52}Bi_{48}$ ribbons using ICP-AES

Element	**Concentration (Atomic %)**
Mn	50.94
+/-	0.25
Bi	49.06
+/-	0.22
	Concentration (Weight %)
Mn	21.44
+/-	0.10
Bi	78.56
+/-	0.35

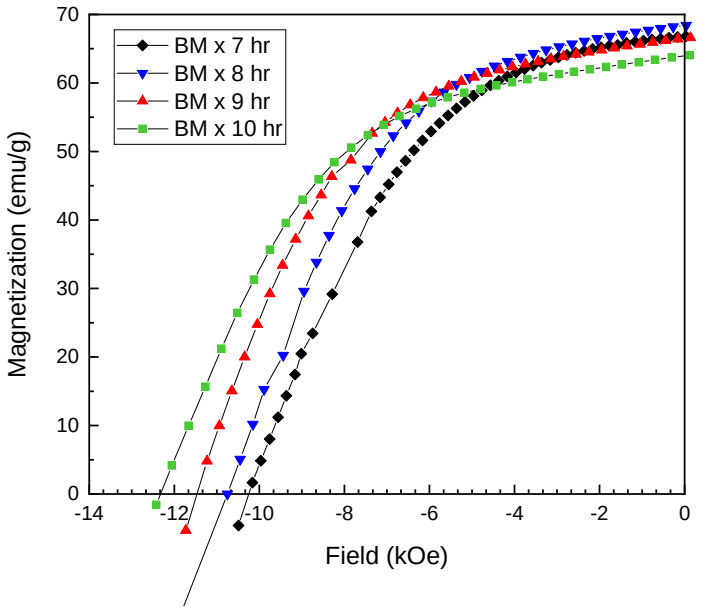

Figure 5. Magnetic properties of $Mn_{52}Bi_{48}$ powders which were ball milled for various times.

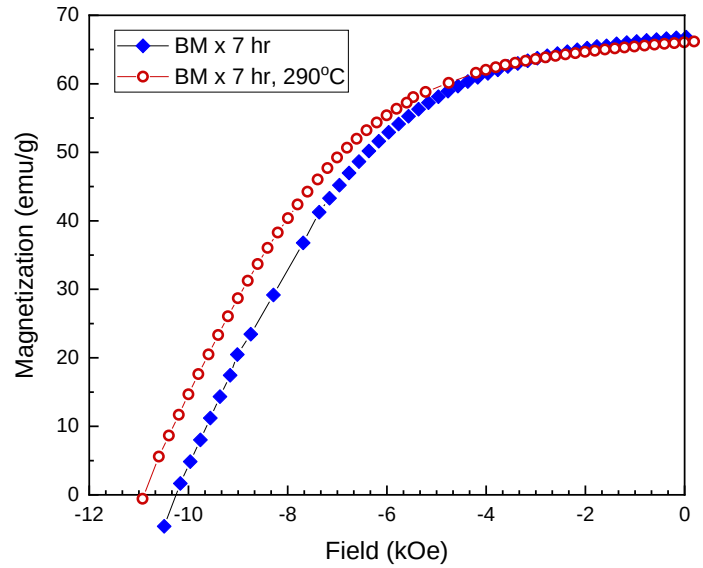

Figure 6. Effects of 290°C annealing treatment on $Mn_{52}Bi_{48}$ ball milled powders. The annealing treatment increases M_S at the cost of a reduction in M_r/M_S.

Table 2. The magnetic properties of ball milled powders aligned in wax, measured at T = 300 K.

Powder Condition	M_S emu g^{-1}	M_r emu g^{-1}	M_r/M_S	H_{ci} kOe	$(BH)_{max}$ MGOe
BM x 7 hr	75.6	66.8	0.88	10.3	12.4
BM x 8 hr	75.5	68.4	0.91	10.8	13.0
BM x 9 hr	74.3	66.5	0.90	11.5	12.5
BM x 10 hr	71.8	63.8	0.89	12.3	11.6
BM x 7 hr, 290°C anneal	78.8	66.1	0.84	10.9	12.4
BM x 10 hr, 290°C anneal	70.7	61.5	0.87	15.0	10.8

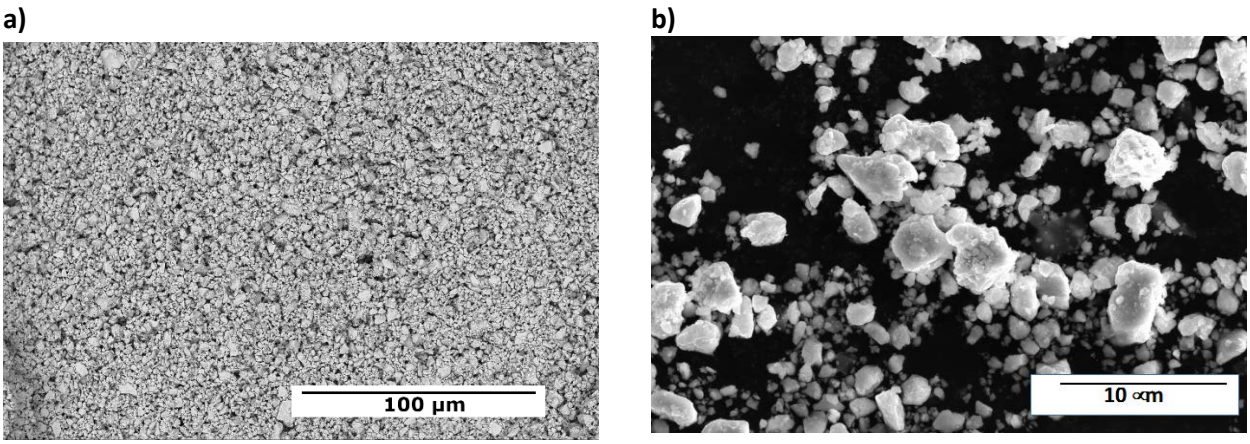

Figure 7. SEM micrograph of MnBi powders after low energy ball milling for 8 hours. Images were taken in backscattered electron imaging mode. Most powder particles fall between the size range of 0.5 µm to 5 µm.

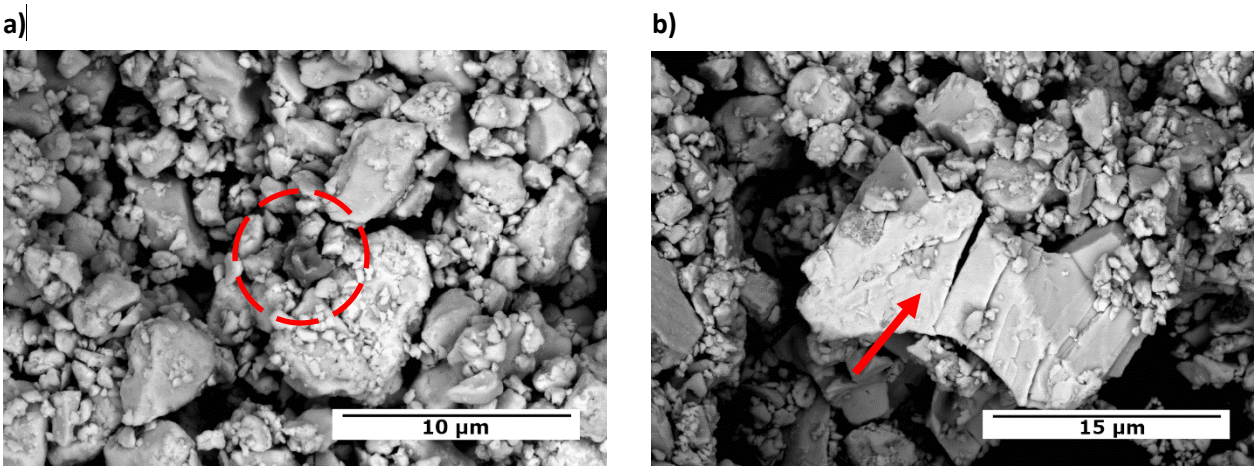

Figure 8. SEM micrograph of Mn and Bi impurities within the ball milled powders. Red circle in image a) highlights a dark, 2 µm grain of elemental Mn. Red arrow in image b) highlights a bright, 20 µm grain of elemental Bi with a faulted surface.

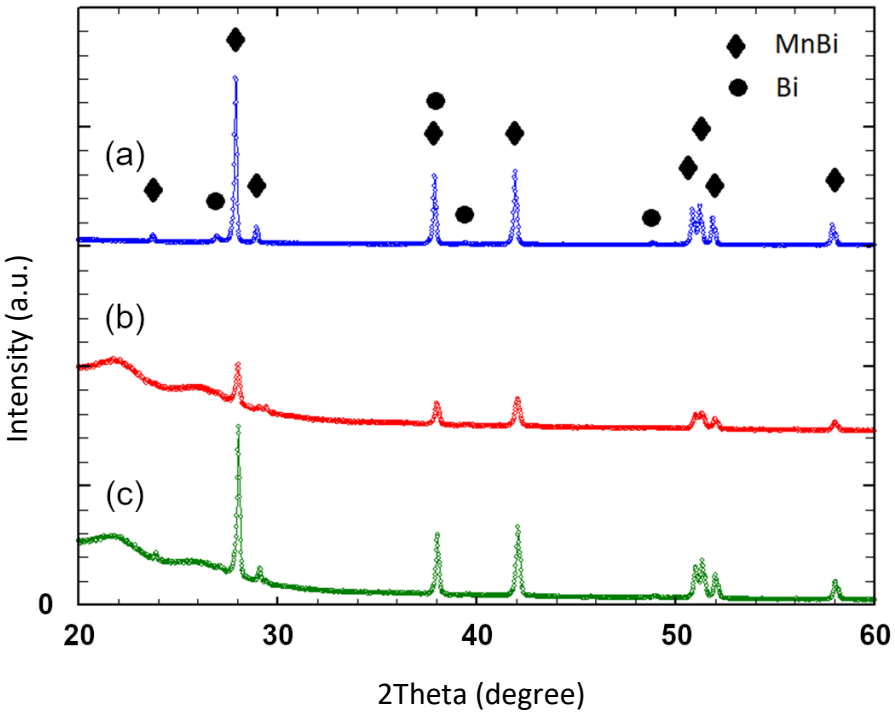

FIGURE 9: XRD patterns for Mn52Bi48 (a) annealed ribbon, (b) ball milled powder, (c) annealed powder.

Table 3. Summary of Rietveld analysis on $Mn_{52}Bi_{48}$ alloy throughout each processing step

Processing step	*a*, *b* (Å)	*c* (Å)	MnBi fraction (wt)	Bi fraction (wt)	Fitting (χ^2)
Annealed ribbon	4.28172(10)	6.11311(17)	0.9687(1)	0.0313(15)	10.620
Ball milled powders	4.28303(20)	6.11004(34)	0.9245(8)	0.0755(68)	3.808
Annealed powders	4.28133(13)	6.11081(21)	0.98501(7)	0.0149(28)	7.399

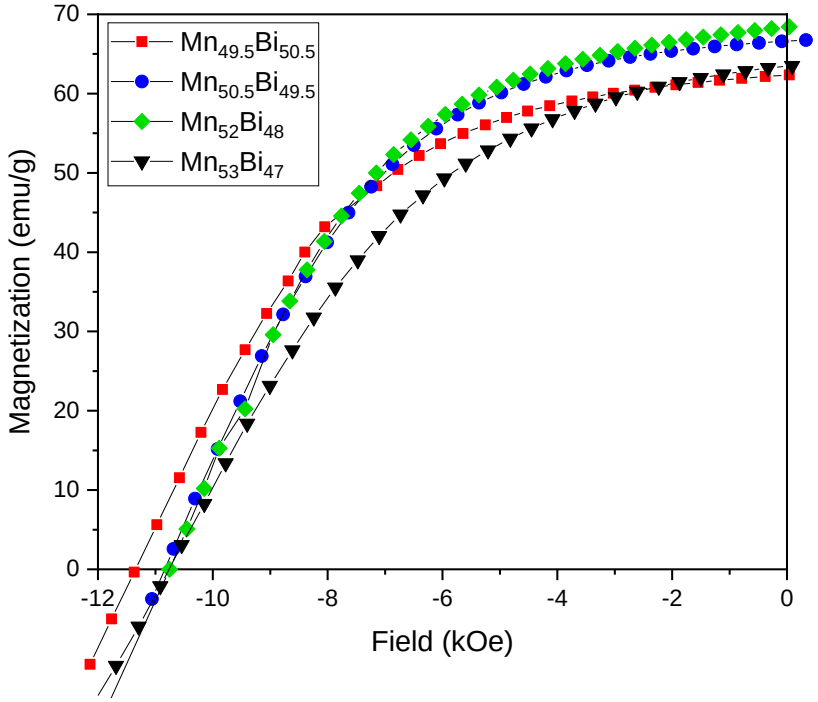

Figure 10. Magnetic properties of $Mn_{100-x}Bi_x$ powders aligned in wax. All compositions were ball milled for 8 hours. Measurements were taken at T = 300 K. The values of coercivity are similar for all alloys, however the values of M_S and M_r are more dependent on chemistry.

Table 4. The magnetic properties of ball milled powders aligned in wax, measured at T = 300 K.

Alloy	M_S (emu g^{-1})	M_r (emu g^{-1})	M_r/M_S	H_{ci} (kOe)	$(BH)_{max}$ (MGOe)
$Mn_{49.5}Bi_{50.5}$	71.9	62.4	0.87	11.4	11.2
$Mn_{50.5}Bi_{49.5}$	74.2	66.6	0.90	10.9	12.6
$Mn_{52}Bi_{48}$	75.5	68.4	0.91	10.8	13.0
$Mn_{53}Bi_{47}$	73.6	63.5	0.86	10.7	11.0

References

[1] X. Guo, X. Chen, Z. Altounian, J.O. Ström-Olsen, Magnetic properties of MnBi prepared by rapid solidification, Phys. Rev. B. 46 (1992) 14578–14582. doi:10.1103/PhysRevB.46.14578.

[2] J. Cui, J.P. Choi, G. Li, E. Polikarpov, J. Darsell, M.J. Kramer, N.A. Zarkevich, L.L. Wang, D.D. Johnson, M. Marinescu, Q.Z. Huang, H. Wu, N. V. Vuong, J.P. Liu, Development of MnBi permanent magnet: Neutron diffraction of MnBi powder, J. Appl. Phys. 115 (2014) 17A743. doi:10.1063/1.4867230.

[3] B.W. Roberts, Neutron Diffraction Study of the Structures and Magnetic Properties of Manganese Bismuthide, Phys. Rev. 104 (1956) 607–616.

[4] T. Chen, Contribution to the equilibrium phase diagram of the Mn–Bi system near MnBi, J. Appl. Phys. 45 (1974) 2358–2360. doi:10.1063/1.1663594.

[5] T. Chen, W.E. Stutius, The Phase Transformation and Physical Properties of the MnBi and Mn1.08Bi Compounds, IEEE Trans. Magn. 10 (1974) 581–586.

[6] K. Oikawa, Y. Mitsui, K. Koyama, K. Anzai, Thermodynamic Assessment of the Bi-Mn System, Mater. Trans. 52 (2011) 2032–2039. doi:10.2320/matertrans.M2011229.

[7] C.P. Wang, W.J. Yu, Z.S. Li, X.J. Liu, A.T. Tang, F.S. Pan, Thermodynamic assessments of the Bi–U and Bi–Mn systems, J. Nucl. Mater. 412 (2011) 66–71. doi:10.1016/J.JNUCMAT.2011.02.021.

[8] A.F. Andresen, W. Hälg, P. Fischer, E. Stoll, The Magnetic and Crystallographic Properties of MnBi Studied by Neutron Diffraction., Acta Chem. Scand. 21 (1967) 1543–1554. doi:10.3891/acta.chem.scand.21-1543.

[9] J. Cui, J.P. Choi, G. Li, E. Polikarpov, J. Darsell, N. Overman, M. Olszta, D. Schreiber, M. Bowden, T. Droubay, M.J. Kramer, N.A. Zarkevich, L.L. Wang, D.D. Johnson, M. Marinescu, I. Takeuchi, Q.Z. Huang, H. Wu, H. Reeve, N. V. Vuong, J.P. Liu, Thermal stability of MnBi magnetic materials, J. Phys. Condens. Matter. 26 (2014). doi:10.1088/0953-8984/26/6/064212.

[10] J. Cui, J.P. Choi, E. Polikarpov, M.E. Bowden, W. Xie, G. Li, Z. Nie, N. Zarkevich, M.J. Kramer, D. Johnson, Effect of composition and heat treatment on MnBi magnetic materials, Acta Mater. 79 (2014) 374–381. doi:10.1016/j.actamat.2014.07.034.

[11] W. Xie, E. Polikarpov, J.P. Choi, M.E. Bowden, K. Sun, J. Cui, Effect of ball milling and heat treatment process on MnBi powders magnetic properties, J. Alloys Compd. 680 (2016) 1–5. doi:10.1016/j.jallcom.2016.04.097.

[12] S. Kim, H. Moon, H. Jung, S.-M. Kim, H.-S. Lee, H. Choi-Yim, W. Lee, Magnetic properties of large-scaled MnBi bulk magnets, J. Alloys Compd. 708 (2017) 1245–1249. doi:10.1016/j.jallcom.2017.03.067.

[13] J.B. Yang, W.B. Yelon, W.J. James, Q. Cai, S. Roy, N. Ali, Structure and magnetic properties of the MnBi low temperature phase, J. Appl. Phys. 91 (2002) 7866. doi:10.1063/1.1451306.

[14] Z. Xiang, T. Wang, S. Ma, L. Qian, Z. Luo, Y. Song, H. Yang, W. Lu, Microstructural evolution and phase transformation kinetics of MnBi alloys, J. Alloys Compd. 741 (2018) 951–956.

doi:10.1016/j.jallcom.2018.01.147.

[15] J. Cao, Y.L. Huang, Y.H. Hou, Z.Q. Shi, X.T. Yan, Z.C. Zhong, G.P. Wang, Microstructure and magnetic properties of MnBi alloys with high coercivity and significant anisotropy prepared by surfactant assisted ball milling, J. Magn. Magn. Mater. 473 (2019) 505–510. doi:10.1016/j.jmmm.2018.10.052.

[16] J.B. Yang, W.B. Yelon, W.J. James, Q. Cai, M. Kornecki, S. Roy, N. Ali, P. L'Heritier, Crystal structure, magnetic properties and electronic structure of the MnBi intermetallic compound, J. Phys. Condens. Matter. 14 (2002) 6509–6519. doi:10.1088/0953-8984/14/25/318.

[17] Y.-C. Chen, S. Sawatzki, S. Ener, H. Sepehri-Amin, A. Leineweber, G. Gregori, F. Qu, S. Muralidhar, T. Ohkubo, K. Hono, O. Gutfleisch, H. Kronmüller, G. Schütz, E. Goering, On the synthesis and microstructure analysis of high performance MnBi, AIP Adv. 6 (2016). doi:10.1063/1.4971759.

[18] S. Kavita, V. V. Ramakrishna, A. Srinivasan, R. Gopalan, Structural and magnetic properties of the low temperature phase MnBi with ball milling, Mater. Res. Express. 3 (2016) 056102. doi:10.1088/2053-1591/3/5/056102.

[19] J.B. Yang, K. Kamaraju, W.B. Yelon, W.J. James, Q. Cai, A. Bollero, Magnetic properties of the MnBi intermetallic compound, Appl. Phys. Lett. 79 (2001) 1846–1848. doi:10.1063/1.1405434.

[20] K. Kanari, C. Sarafidis, M. Gjoka, D. Niarchos, O. Kalogirou, Processing of magnetically anisotropic MnBi particles by surfactant assisted ball milling, J. Magn. Magn. Mater. 426 (2017) 691–697. doi:10.1016/j.jmmm.2016.10.141.

[21] N. V. Rama Rao, A.M. Gabay, W.F. Li, G.C. Hadjipanayis, Nanostructured bulk MnBi magnets fabricated by hot compaction of cryomilled powders, J. Phys. D. Appl. Phys. 46 (2013). doi:10.1088/0022-3727/46/26/265001.

[22] Y.S. Cho, C.C. Koch, Mechanical milling of ordered intermetallic compounds: the role of defects in amorphization, J. Alloys Compd. 194 (1993) 287–294. doi:10.1016/0925-8388(93)90013-D.

[23] C.C. Koch, J.D. Whittenberger, Mechanical milling/alloying of intermetallics, Intermetallics. 4 (1996) 339–355. doi:10.1016/0966-9795(96)00001-5.

[24] F. Yin, N. Gu, T. Shigematsu, N. Nakanishi, Sintering Formation of Low Temperature Phase MnBi and Its Disordering in Mechanical Milling, 1996.

[25] H. Kronmüller, J.B. Yang, D. Goll, Micromagnetic analysis of the hardening mechanisms of nanocrystalline MnBi and nanopatterned FePt intermetallic compounds, J. Phys. Condens. Matter. 26 (2014). doi:10.1088/0953-8984/26/6/064210.

[26] X. Guo, A. Zaluska, Z. Altounian, J.O. Ström-Olsen, The formation of single-phase equiatomic MnBi by rapid solidification, J. Mater. Res. 5 (1990) 2646–2651.